Talanta 276 (2024) 126216

Contents lists available at ScienceDirect

Talanta

journal homepage: www.elsevier.com/locate/talanta

Native characterization and QC profiling of human amniotic mesenchymal stromal cell vesicular fractions for secretome-based therapy

Valentina Marassi [a,b], Giampiero La Rocca [c], Anna Placci [a], Alexandra Muntiu [d], Federica Vincenzoni [e,f], Alberto Vitali [d], Claudia Desiderio [d], Tullia Maraldi [g], Francesca Beretti [g], Eleonora Russo [c], Vitale Miceli [h], Pier Giulio Conaldi [h], Andrea Papait [f,i], Pietro Romele [j], Anna Cargnoni [j], Antonietta Rosa Silini [j], Francesco Alviano [k], Ornella Parolini [f,i], Stefano Giordani [a], Andrea Zattoni [a,b], Pierluigi Reschiglian [a,b], Barbara Roda [a,b,*]

[a] Department of Chemistry G. Ciamician, University of Bologna, Italy
[b] byFlow srl, Bologna, Italy
[c] Department of Biomedicine, Neurosciences and Advanced Diagnostics, University of Palermo, 90127, Palermo, Italy
[d] Istituto di Scienze e Tecnologie Chimiche "Giulio Natta", Consiglio Nazionale delle Ricerche, 00168, Rome, Italy
[e] Dipartimento di Scienze Biotecnologiche di Base, Cliniche Intensivologiche e Perioperatorie, Università Cattolica del Sacro Cuore, 00168, Rome, Italy
[f] Fondazione Policlinico Universitario A. Gemelli IRCCS, 00168, Rome, Italy
[g] Department of Biomedical, Metabolic and Neural Sciences, University of Modena and Reggio Emilia, 41125, Modena, Italy
[h] Research Department, IRCCS ISMETT (Istituto Mediterraneo per i Trapianti e Terapie ad alta Specializzazione), 90127, Palermo, Italy
[i] Department of Life Science and Public Health, Università Cattolica del Sacro Cuore, 00168, Rome, Italy
[j] Centro di Ricerca E. Menni, Fondazione Poliambulanza Istituto Ospedaliero, 25124, Brescia, Italy
[k] Department of Biomedical and Neuromotor Science, University of Bologna, Bologna, Italy

ARTICLE INFO

Handling editor: Qun Fang

Keywords:
Extracellular vesicles
Mesenchymal stromal cells (MSC) secretome
Hollow-fiber flow field-flow fractionation
Multi-angle light scattering
LC-MS proteomics

ABSTRACT

Human amniotic mesenchymal stromal cells (hAMSCs) have unique immunomodulatory properties making them attractive candidates for regenerative applications in inflammatory diseases. Most of their beneficial properties are mediated through their secretome. The bioactive factors concurring to its therapeutic activity are still unknown. Evidence suggests synergy between the two main components of the secretome, soluble factors and vesicular fractions, pivotal in shifting inflammation and promoting self-healing. Biological variability and the absence of quality control (QC) protocols hinder secretome-based therapy translation to clinical applications. Moreover, vesicular secretome contains a multitude of particles with varying size, cargos and functions whose complexity hinders full characterization and comprehension.

This study achieved a significant advancement in secretome characterization by utilizing native, FFF-based separation and characterizing extracellular vesicles derived from hAMSCs. This was accomplished by obtaining dimensionally homogeneous fractions then characterized based on their protein content, potentially enabling the identification of subpopulations with diverse functionalities.

This method proved to be successful as an independent technique for secretome profiling, with the potential to contribute to the standardization of a qualitative method. Additionally, it served as a preparative separation tool, streamlining populations before ELISA and LC-MS characterization. This approach facilitated the categorization of distinctive and recurring proteins, along with the identification of clusters associated with vesicle activity and functions. However, the presence of proteins unique to each fraction obtained through the FFF separation tool presents a challenge for further analysis of the protein content within these cargoes.

1. Introduction

Mesenchymal stromal cells (MSC) have attracted increasing interest for their possible application in the treatment of diseases in which the immune system is dysregulated [1–3]. It is increasingly more evident that MSC are able to exert their therapeutic action through the factors

* Corresponding author. Department of chemistry G. Ciamician, University of Bologna, Italy.
E-mail address: barbara.roda@unibo.it (B. Roda).

https://doi.org/10.1016/j.talanta.2024.126216
Received 18 December 2023; Received in revised form 9 April 2024; Accepted 5 May 2024
Available online 8 May 2024

they release which are contained in their secretome [2,4–6]. Specifically, two components have been identified in the secretome, namely the extracellular vesicles (EVs) and the secreted factors not enclosed by vesicles, such as cytokines, chemokines, and growth factors [7,8]. More recently, EVs have risen to prominence as a therapeutic approach in regenerative medicine due to their potential to serve as cell exchange vehicles not only for miRNAs, but also for proteins, lipids, and soluble factors, and due to their easier management/storage and higher safety (i.e., lack of tumorigenicity) compared to cell-based therapy, thus potentially maintaining the same therapeutic properties of the cell of origin [9]. Among the various MSCs, those isolated from the amniotic membrane (hAMSC), and their secretome, have been shown to exert a strong immunomodulatory actions both *in vitro* and *in vivo*, and to induce therapeutic effects in various preclinical models of disease [10–17]. EVs obtained from hAMSC have been recently reported to possess miRNAs characteristic of immunomodulatory and chondroprotective actions [18,19].

However, the use of MSC conditioned media in toto as well as EVs shows some limitations. The main issues are related to the characterization of bioactive components and standardization of secretome products in terms of conditioned media formulation. Indeed, gender, donor age, and phenotype are among the factors influencing the secretome products. Moreover, the preparation methods can also impact on the biological effects of secretome. A comprehensive characterization of the secretome is mandatory to guarantee reproducibility of the treatments and to identify the mechanisms of therapeutic effects [20]. Approaches based on multiple techniques such as immunoassays, flow cytometry, liquid chromatography, *in vitro* biological tests and advanced technologies such as next-generation-sequencing, are applied to the study of secretome to identify potential molecular mechanisms responsible for the observed therapeutic/biological effect [21–24]. Despite advancements, there is an ongoing need for the development of methods that can accurately, efficiently, and reproducibly characterize the biomolecular content of MSC or other cell-based secretomes. Specifically, understanding the composition of extracellular vesicles (EVs) in the secretome and their potential role as carriers for bioactive molecules involved in paracrine signaling remains an open and critical issue for comprehending its regenerative potential. Conventional methods commonly used for EVs isolation include ultracentrifugation-based methods, size-based methods (size-exclusion chromatography and ultrafiltration), precipitation, and immunoaffinity capture [25,26]. Nevertheless, the predominant challenge in characterizing EVs arises from their dimensional heterogeneity. The primary obstacle indeed lies in the absence of efficient and versatile systems capable of isolating homogeneous fractions of EVs with high efficiency and a high degree of purity.

Among separative techniques for the analysis of complex biological samples, the size-based separation technique Field-Flow Fractionation (FFF) represents an emerging tool operating in soft conditions with complete maintenance of the native properties of analytes. FFF has already been applied to the analysis of complex samples including EVs from cell lines and biological samples [27–31]. FFF was also used to address the complexity of EVs from a cancer cell line through the study of their proteomic and genomic profile, and biophysical properties [32]. The low-volume, tubular variant of FFF, namely hollow-fiber flow field-flow fractionation (HF5), shows intrinsic additional advantages: the reduced channel volume and operation flowrates, the low dilution of fractionated analytes, and the potentially disposable use with minimal sample handling [33–35]. Through an HF5 method employing UV, fluorescence and Laser Scattering as detectors, we recently published a characterization in terms of size, abundance and DNA/protein content of subpopulations of membrane-derived vesicles from culture medium of murine myoblasts; and the purification of fractions for further biological characterization, and the enrichment of serum-derived EVs prior to microfluidic biosensing with diagnostic purposes [36,37]. In this study, a method based on HF5 was developed and applied for the first time to the pre-proteomic isolation of homogeneous EVs fractions of the hAMSC secretome to obtain their comprehensive characterization by combination of the top-down and bottom-up approaches.

This method allowed us to identify 7 vesicular fractions representative of the great heterogeneity existing in the EVs compartment of the hAMSC secretome and presenting fraction-specific protein profiles. The differences among fractions were evaluated by their proteomic profile using a Liquid Chromatography-high resolution Mass Spectrometry (LC–MS) platform.

2. Materials and Methods

2.1. hAMSCs isolation, expansion, and secretome production

The study was conducted in accordance with the Declaration of Helsinki, and informed consent was obtained following the guidelines defined by the Brescia Provincial Ethics Committee (number NP 2243, January 19, 2016). Human term placentas were collected from healthy women and processed within 8 h of birth. hAMSCs were isolated as previously described [38].

To obtain hAMSC at passage 1 (hAMSC-P1), freshly isolated cells were plated in flasks (Euroclone) at a density of 10,000 cells/cm^2 in CHANG Medium-C (Irvine Scientific) supplemented with 2 mM L-glutamine (Euroclone) and 100 U/ml penicillin and 100 μg/ml streptomycin (herein referred to as P/S, both from Euroclone) at 37 °C and 5 % CO_2. Upon reaching subconfluency, adherent cells were washed in PBS, detached with 0.25 % trypsin EDTA (Merck) and then sub-cultured in 24-well plates (Euroclone) at a density of 500,000 cells/well in 0.5 mL of DMEM-F12 Medium (Life Technologies) supplemented with 2 mM L-glutamine and P/S [39]. At the end of a 5-day culture, conditioned medium of human amniotic mesenchymal stromal cells (CM-hAMSC) was collected and centrifuged at 300×*g*.

Before subculturing for conditioned medium preparation, hAMSCs underwent phenotypic characterization after isolation (p0). These cells fulfilled the essential criteria for mesenchymal stromal cells (MSCs), demonstrating positive expression for mesenchymal markers CD13 (97.7 ± 1.6 %; mean ± SD), CD73 (88.3 ± 6.4 %), CD90 (94.8 ± 7.4 %), while lacking the expression of hematopoietic markers such as CD45 (1.8 ± 1.0 %), CD66b (0 %), and the epithelial marker CD324 (1.7 ± 1.0 %) [38,40–42].

2.2. Isolation and characterization of EVs

The serum-free medium conditioned by hAMSC (CM-hAMSC) was then centrifuged for 20 min at 17,500×*g* and lastly ultracentrifuged at 120,000×*g* for 90 min at 4 °C to pellet the EV. Both size and concentration of EV were determined by nanoparticles tracking analysis (NTA) in a NanoSight NS3000 (Malvern Instruments Ltd, Malvern, UK). Briefly, the samples were diluted 1:500 in PBS to reach optimal concentration for instrument linearity, and the data were analysed with NTA software (version 3.1). Five recordings of 60 s at 25 frames per second were performed.

2.3. HF5-UV-FLD-MALS

2.3.1. Instrumental setup

HF5 analyses were performed using an Agilent 1200 HPLC system (Agilent Technologies, Santa Clara, CA, USA) consisting in a degasser, an isocratic pump, with an Agilent 1100 DAD UV/Vis spectrophotometer combined with an Eclipse® DUALTEC separation system (Wyatt Technology Europe, Dernbach, Germany). The scheme of the HF5 cartridge, its assembly, and the modes of operation of the Eclipse® DUALTEC system have already been described elsewhere [43]. The hollow fiber was a polyethersulfone (PES) fiber, with0.8 mm ID, 1.3 mm OD, and 10 kDa Mw cut-off, corresponding to an average pore diameter of 5 nm. The ChemStation version B.04.02 (Agilent Technologies) and Wyatt Eclipse

@ ChemStation version 3.5.02 (Wyatt Technology Europe) plugin was used to handle separation methods. An 18-angle multiangle light scattering detector model DAWN HELEOS (MALS, Wyatt Technology Corporation, Santa Barbara, CA, USA) operating at a wavelength of 658 nm, was used to measure the radius of particles in solution. ASTRA® software version 6.1.7 (Wyatt Technology Corporation) was used to handle signals from the detectors (MALS and UV) and to compute the sample Rg values.

2.3.2. Fractionation method and size analysis

An HF5 method is composed of four steps: focus, focus–injection, elution and elution–injection. During focus the mobile phase enters from both inlet and outlet and stabilizes; during focus–injection, the flow settings remain unvaried while the sample is introduced into the channel through the inlet and focalized in a narrow band. Then, in the elution step, the flow of mobile phase enters the channel inlet and part of it comes out transversely (cross-flow, Vx), while the rest (channel flow, Vc) reaches the detectors; lastly, during elution–injection, no cross-flow is applied allowing for any remaining sample inside the channel to be released; also, the flow is redirected in the injection line as well to clean it before the next injection. The flow conditions for the developed HF5 method are as follows. The detector flow was kept constant at 0.35 ml/min. During focusing, focus flow was kept at 0.8 ml/min for 0.5 min, then focus injection carried on with the same parameters for 2.5 min. Subsequently, elution was performed with two subsequent gradients: 0.5 to 0.05 ml/min in 5 min, and 0.05 to 0.03 ml/min in 14 min. The crossflow was then kept at zero for additional 6 min and the injector was washed out for additional 2 min. Longitudinal flow is indicated as Vc, while cross/focus flow as Vx. Recovery was calculated as FocusFIA/FIA area ratio %, the two methods being a filtrating, non-separating injection and a non-filtrating, non-separating injection. UV signal at 280 nm was the signal analysed leading to a recovery >95 % for injections of BSA standard solutions (15 μg injections, n = 3) and >89 % for secretome samples (only a lower volume of 8 μL was available for injection given the low availability of the sample).

Repeatability and reproducibility were assessed on retention times and signal intensity both intra- and inter-day (n = 3) for protein standard BSA. The deviations (15 μg injections) were of less than 1 % and 2 % in terms of retention time and signal intensity, respectively. LOD (three-sigma) and LOQ (ten-sigma) for BSA were calculated to be 0.08 μg and 0.11 μg. The developed method followed the harmonized guideline ICHQ2R1 and ISO/TS 21362 criteria [44–46].

A volume of 30 μL previously dilluted 1:2 in PBS, was injected for sample characterization.

Based on FFF theory retention time is inversely proportional to the hydrodynamic diffusion coefficient of the analyte and, consequently, to its Mr or hydrodynamic radius (*R*h) using Stokes-Einstein's equation [47,48]. The hydrodynamic radii were calculated according to FFF theory with the software ISIS (Wyatt Technology Europe) for method size calibration, whose results were also confirmed by the correspondence between calculated and experimental retention times of a protein mix (BSA:IgG 2:1) [49].

MALS was used to determine colloidal size. Being this a direct measurement, it is considered an absolute detector since it does not require external calibration to compute radius values. the determination of particle root mean square radius of gyration (Rg) is performed by measuring the net intensity of light scattered by such particles at a range of fixed angles [50].

2.3.3. Protein quantification

UV absorbance and FLD signals for proteins were measured to assess protein concentration at a specific time point. Protein content of EVs fractions was evaluated by on-line measuring the fluorescence produced at 340 nm upon excitation at 280 nm during the separation method. Known quantities (10–80 μg) of a standard protein (BSA, Sigma-Aldrich) were submitted to the same separation method to calibrate for protein quantification: fluorescence peak areas were plotted against injected amount and areas were interpolated to obtain their relative protein amount.

2.4. ELISA assays

CD9, CD63, CD81, IL-6, IL-10, TGFβ1, pentraxin 3 (Cusabio, Huston, TX, USA), IDO (MyBioSource, San Diego, CA, USA) and HGF (Boster Biological Technology, Pleasanton, CA, USA) were quantified in the lysed of total and/or fractionated EVs. Briefly, EVs were lysed using a lysis buffer (20 mM Tris-Cl, pH 7.0; 1 % Nonidet P-40; 150 mM NaCl; 10 % glycerol; 10 mM EDTA; 20 mM NaF; 5 mM sodium pyrophosphate; and 1 mM Na_3VO_4) and freshly added to a pro-tease inhibitor cocktail (Sigma Aldrich) and *para*-nitrophenylphosphate (Sigma Aldrich) at a ratio of 1:3 (vol:vol) followed by 3 cycles of freeze and thaw; the seven fractions of EVs were lysed through three cycle freeze and thaw, and 20 cycles of sonication. ELISA assays for the different antigens were performed using 3 ml (1 μg of total lysed EVs and 100 μl of lysed fractions, according to the manufacturer's protocol).

2.5. Statistical analysis

The experiments were performed in triplicate (biological replicates). For quantitative comparisons, the values were reported as the mean ± SEM based on a triplicate analysis for each sample. To test the significance of the observed differences amongst the study groups, a one-way ANOVA with a Bonferroni post hoc test or a Student's *t*-test was applied. A *p*-value <0.05 was considered to be statistically significant. The statistical analysis and plot layout were obtained by using GraphPad Prism® release 6.0 software.

2.6. Chemicals

Urea, Trizma base, Iodoacetamide (IAA), D,L-dithiothreitol (DTT), Protease Inhibitor cocktail (PIC), acetone and ammonium bicarbonate (AMBIC) were from Sigma-Aldrich (St. Louis, MO, USA). Trypsin enzyme (Gold MS Grade) was from Promega (Madison, WI, USA). Water, formic acid (FA) and Acetonitrile (ACN) (all LC-MS grade) and Hydrochloric acid fuming 37% were from Merck (Darmstadt, Germany).

2.7. Proteomic analysis

2.7.1. Extracellular vesicle fractions pretreatment

The seven fractions of extracellular vesicles plus their total fraction, purified and lyophilized, were lysed in 200 μL urea lysis buffer solution (Urea 8 M in 0.1 M Tris/HCl, pH 8.5) under sonication (15x cycles, 30s on, 30s off) (Sonica Soltec, Ultrasonic cleaner, Milano, Italy) [51]. The various fractions were finally gently vortexed to allow the resolubilization of their content. A Filter Aided Sample Preparation (FASP) method with 10 kDa membrane filter cut-off (Millipore) [52,53], was applied for protein digestion protocol. Briefly, the entire volume of each sample, corresponding to 200 μL, was transferred to the filter device for protein digestion and centrifuged at 14000 rpm for 15 min. The filter device supernatant underwent overnight protein digestion using trypsin enzyme 1:100 (v/v) after disulfide bridge reduction and alkylation by treatment with 8 mM DTT incubation in Urea Buffer solution and carbamide methylation by 50 mM iodoacetamide (IAA) in Urea Buffer solution, respectively.

After digestion, the resulting protein digests of each fraction were collected by centrifugation from FASP device and lyophilized. Before LC-MS analysis the lyophilized samples were redissolved in 0.1 % (v/v) FA solution volumes variable for each fraction based on their estimated total protein content before lysis by HF5 analysis, as described in the previous paragraph. All samples were analysed in order to inject in each run of duplicate LC-MS analysis 800 ng of total proteins with the exception of fraction 1 and 7, where the injected protein content was

200 and 64 ng, respectively, due to their lower protein content.

The filtered volume, corresponding to the fraction with molecular weight <10 kDa, was collected for the characterization of peptides and small proteins in their intact form after addition of protease inhibitor cocktail (PIC, 1:20 v/v, of 20x concentrated solution) and overnight protein precipitation with 6x volumes of cold acetone at −80 °C. The resulting pellet was redissolved in 0.1 % (v/v) FA water solution for LC-MS analysis.

2.7.2. UHPLC-ESI-Orbitrap Elite analysis

LC-ESI-MS/MS analyses were performed in duplicate on UltiMate 3000 RSLCnano System coupled to Orbitrap Elite MS detector with EASY-Spray nanoESI source (Thermo Fisher Scientific, Waltham, MA, USA) and Thermo Xcalibur 2.2 computer program (Thermo Fisher Scientific) for instrumental operation and data acquisition. Chromatographic separation was performed on EASY-Spray PepMap C18 column (15 cm in length x 50 μm of internal diameter (ID), 2 μm particles, 100 Å pore size) (Thermo Fisher Scientific) in coupling to Acclaim PepMap100 nano-trap cartridge (C18, 5 μm, 100 Å, 300 μm i.d. x 5 mm) (Thermo Fisher Scientific). Separation was performed at 40 °C in gradient elution, at mobile phase flow rate of 0.3 μL/min, using aqueous FA solution (0.1 %, v/v) as eluent A and ACN/FA solution (99.9:0.1, v/v) as eluent B as following: (i) 5 % B (7 min), (ii) from 5 % to 35 % B (113 min), (iii) from 35 % B to 99 % (2 min), (iv) 99 % B (3 min), (v) from 99 % to 1.6 % B (2 min), (vi) 1.6 % B (3 min), (vii) from 1.6 % to 78 % B (3 min), (viii) 78 % B (3 min), (ix) from 78 % to 1.6 % B (3 min), (x) 1.6 % B (3 min), (xi) from 1.6 % to 78 % B (3 min), (xii) 78 % B (3 min), (xiii) from 78 % B to 5 % B (2 min), (xiv) 5 % B (20 min). The injection volume was 5 μL. The Orbitrap Elite instrument was operated in positive ionization mode at a 60,000 full scan resolution in 350–2000 *m/z* acquisition range, performing MS/MS fragmentation by collision-induced dissociation (CID, 35 % normalized collision energy) of the 20 most intense signals of each MS spectrum in Data-Dependent Scan (DDS) mode. The minimum signal was set to 500.0, the isolation width to 2 *m/z* and the default charge state to +2. MS/MS spectra acquisition was performed in the linear ion trap at normal scan rate. For top-down analysis, the acquisition of MS/MS spectra was performed at resolution of 60,000 and setting isolation width to 5 *m/z*.

2.7.3. Data analysis

Raw data of the dataset were analysed using the HPLC-MS apparatus management software (Xcalibur 2.0.7 SP1, Thermo Fisher Scientific), by means of Proteome Discoverer 1.4 software (version 1.4.1.14, Thermo Fisher Scientific) and searched against the Swiss-Prot reviewed *Homo sapiens* database (Uniprot, downloads release 2022_02). The results of the protein identification were filtered, according to the Human Proteome Project (HPP) recommendations [54], for high confidence, characterization of at least 2 peptides for protein, minimum peptide length 9 amino acids and peptide rank 1 for the bottom-up approach; while to identify whole peptides naturally present in extracellular vesicles for top-down approach (<10 kDa), the results were filtered for high confidence and for peptide rank 1. Gene ontology (GO) analysis and classification was performed by Reactome (https://reactome.org) [55] and Protein Analysis Through Evolutionary Relationships (PANTHER, http://www.pantherdb.org) [56] using Fisher's Exact test type with false discovery rate (FDR) correction. Functional protein interaction networks were analysed by means of STRING tool (https://string-db.org) [57] in the highest confidence. Sample data grouping analysis was performed by Venn diagram tool (http://bioinformatics.psb.ugent.be/webtools/Venn/).

3. Results and discussion

3.1. EVs characterization

To exclude biological variability, the secretome derived from two hAMSC donors were pooled, and extracellular vesicles were obtained through ultracentrifugation. Two pools so obtained, thus deriving from 4 donors in total, were used to perform all analyses. Fig. 1A shows a representative graph of nanoparticle tracking analysis (NTA) performed on hAMSC-EVs. The median diameter of the particles was 172.3 nm with a mode of 150.8 nm, compatible with the characteristics of micro-vesicles and exosomes.

The number of vesicles obtained from the CM was around 2,6-5 × 10^9particles/10^6 cells. A preliminary evaluation of exosome markers and a confirmation of the vesicular nature of the isolated sample was performed through quantification of immunomodulating molecules, shown in Fig. 1B.

Coherently with what reported in literature and in Exocarta database for other types of perinatal MSCs, immunomodulating molecules, namely, HGF, IL-6, IL-10, TGFβ1 resulted expressed in hAMSC-EVs, but not in the non-conditioned medium, as expected.

3.2. EVs fractionation

The samples were then processed and characterized on-line through the HF5-multidetection platform, and collected fractions were submitted to offline immunoassays and proteomic analysis.

First, the HF5 analytical platform was investigated for the fractionation of hAMSC-EVs. Parameters and protocols were established and optimized with the aim of obtaining size-homogeneous fractions to be further characterized offline. Indeed, HF5 allows to resolve different particle populations according to hydrodynamic size in their native form, and to characterize them by means of non-destructive method of detection, i.e., absorption, fluorescence, and size/molar mass ratio. In our case, the employed detectors were a UV diode array detector (DAD), a spectrofluorometer (FLD) tuned on proteins intrinsic fluorescence (excitation at 280 nm and emission at 340 nm) and a multiangle light scattering (MALS), the latter providing a direct measurement of the gyration radius of the eluted particles.

Fig. 2A shows a representative fractographic profile obtained from the LS signal at 90° and the calculated radius of gyration (Rg) of the eluted species (dotted distribution) obtained through MALS detection. The method size-calibration obtained from FFF theory (see see Materials and Methods) expressed as hydrodynamic radius (Rh) is also overlaid.

LS analysis reveals one main band eluted between 11 and 26 min, corresponding to a gyration radius between 20 and 200 nm and a hydrodynamic radius between 20 and 150 nm. By correlating these parameters, it is possible to obtain the Rg/Rh ratio, namely the shape factor, corresponding to 1 for hollow spherical species, values inferior to 1 for core-shell structures, and values > 1 for elongated structures [58]. The shape factors obtained for particles eluted in the main band ranged from 0.8 at 11 min, to 0.9–1 along the band, and increased to 1.2 towards the tail, in accordance with the presence of particles carrying cargo (with a shape ratio closer to that a solid sphere) and aggregated species at a higher retention times, where some vesicles could degrade and rupture, a tendency we already observed for LEVs [59]. At 28 min, the crossflow was released allowing for totally retained particles to be eluted. In this case, the signal was close to zero, showing that no higher order aggregation, which indicates sample degradation, occurred.

More information can be gathered by observing the corresponding UV profile (Fig. 2B) set at 280 nm. This wavelength is typical for aromatic rings of peptides composing proteins (Trp, Phe, Tyr) but is not unique for those species and can be used as a more general detection wavelength. In fact, the UV signal highlighted two earlier peaks at 7 and 9 min respectively, whose size cannot be estimated by MALS since their size is inferior to its lower limit (10 nm). The fluorescence signal, selectively tuned on protein emission, only detected the second peak, and the absorption spectrum confirmed that the species at 7 min corresponded to free DNA (absorption max at 260 nm) while the second to free proteins (not shown).

We identified seven fractions (F1–F7) of equal volume and collection

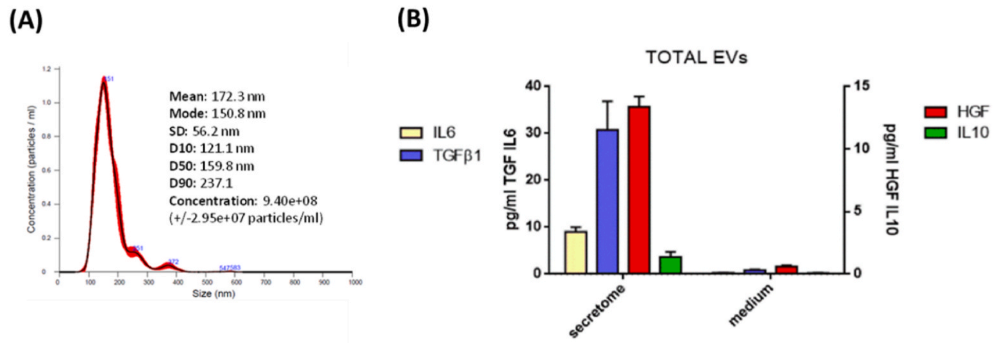

Fig. 1. EVs characteristics. (**A**) Representative nanoparticle tracking analysis (NTA) performed on EVs suspension with Nanosight. (**B**) ELISA analysis of EVs derived from CM and medium alone for TGFβ1, IL-6 and HGF, IL-.10 on the lysates of isolated EVs (N = 3).

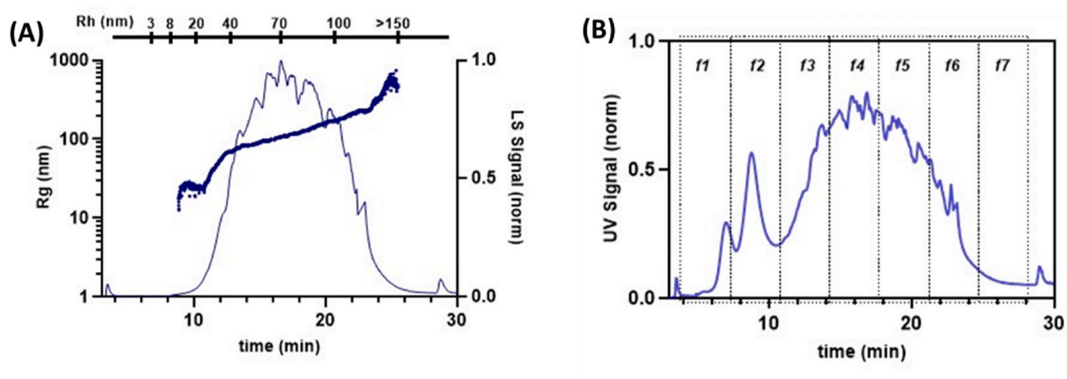

Fig. 2. (A) Representative fractogram (LS signal at 90°) and gyration radii for hAMSC-EV sample. (B) F1–F7 collected fractions (UV signal at 280 nm).

time (Fig. 2B), corresponding to the entire separation profile and balancing operational needs (size-homogeneous fractions) and sample amount to be collected (to be enough for offline characterization). F1 represents the void peak. Based on dimensional distribution values and on the intensity of UV and fluorescence signals discussed above we can assert that F2 is a mixture of proteins and nanoparticles debris, while in F3–F6 all particles in the EVs typical size range are eluted, with F3 and F4 the most abundant fractions. F7 was composed by a very low amount of aggregates with much larger sizes.

The protein content of each fraction was determined by fluorescence following calibration with a standard protein (see Materials and Methods), due to the higher specificity of detection towards proteins with respect to UV absorption, however the different spectroscopical behaviours of the proteins present on particles surface, across the EVs membranes and in the cargo that could occur has to be taken into account. The obtained results, indicating a total protein content of the EVs fractions between 0,5 and 8,8 μg (Table 1), and indicating F3 and F4 as the fractions containing the highest amount of proteins, allowed to plan the subsequent analytical steps by ELISA and mass spectrometry analysese, considering that fluorescence calibration featured as a reliable and, most of all, quick method to quantify protein content in these samples.

In summary, these results indicate that HF5 allows the selection of homogeneous subpopulations in the dimensional range of EVs directly from conditioned medium as well as the characterization of particle population (spherical, loaded, aggregated/unaggregated) separated from free proteins and NA and collected with a quantifiable protein content, facilitating direct downstream investigations.

Table 1
Proteins content of F1–F7.

	F1	F2	F3	F4	F5	F6	F7	tot
Protein (μg)	0.5	8.8	4.8	5.5	4.4	4.4	0.9	29.3

3.3. ELISA of EVs

To explore the real nature of nanoparticles collected in each fraction, they were analysed for the content of expressed vesicle markers. The group of tetraspanins CD9, CD63, and CD81 are the most common EV-associated markers reported in the literature, but they are in fact heterogeneously expressed across EVs: indeed, EV subpopulations exist with unique tetraspanin density and multiplexing even from a single cell source [60].

The presence of these typical exosome markers was verified by ELISA tests performed on fractions obtained from hAMSC-EVs (Fig. 3a) and the results confirmed the EVs features of the particles fractionated from the hAMSC secretome. The results are presented in Fig. 3 as Relative % yield in y-axis of each marker analysed to compare their distribution among fractions.

Whereas no significant variations for CD9 and CD63 were observed between the EVS fractions, an increase of CD81 was instead observed in F4–F6. As discussed in the previous paragraph, F4–F6 are the fractions mainly consisting of whole particles, consequently the ELISA results confirmed the EVs nature of fractionated particles from the hAMSC secretome. Although the analysed parameters are well-known EV-associated markers, their expression is reported to change with EV subclass, size, and source; and they are not ubiquitous on EVs [60,61].

Functional properties of fractionated EVs were studied by ELISA for immunomodulating factors, namely TGFβ1, HGF, IL-10, IDO, IL-6 and pentraxin 3 (Fig. 3b). Increased values for TGFβ1 from F4 to F6 were observed, while no variations were detected for IDO, HGF and

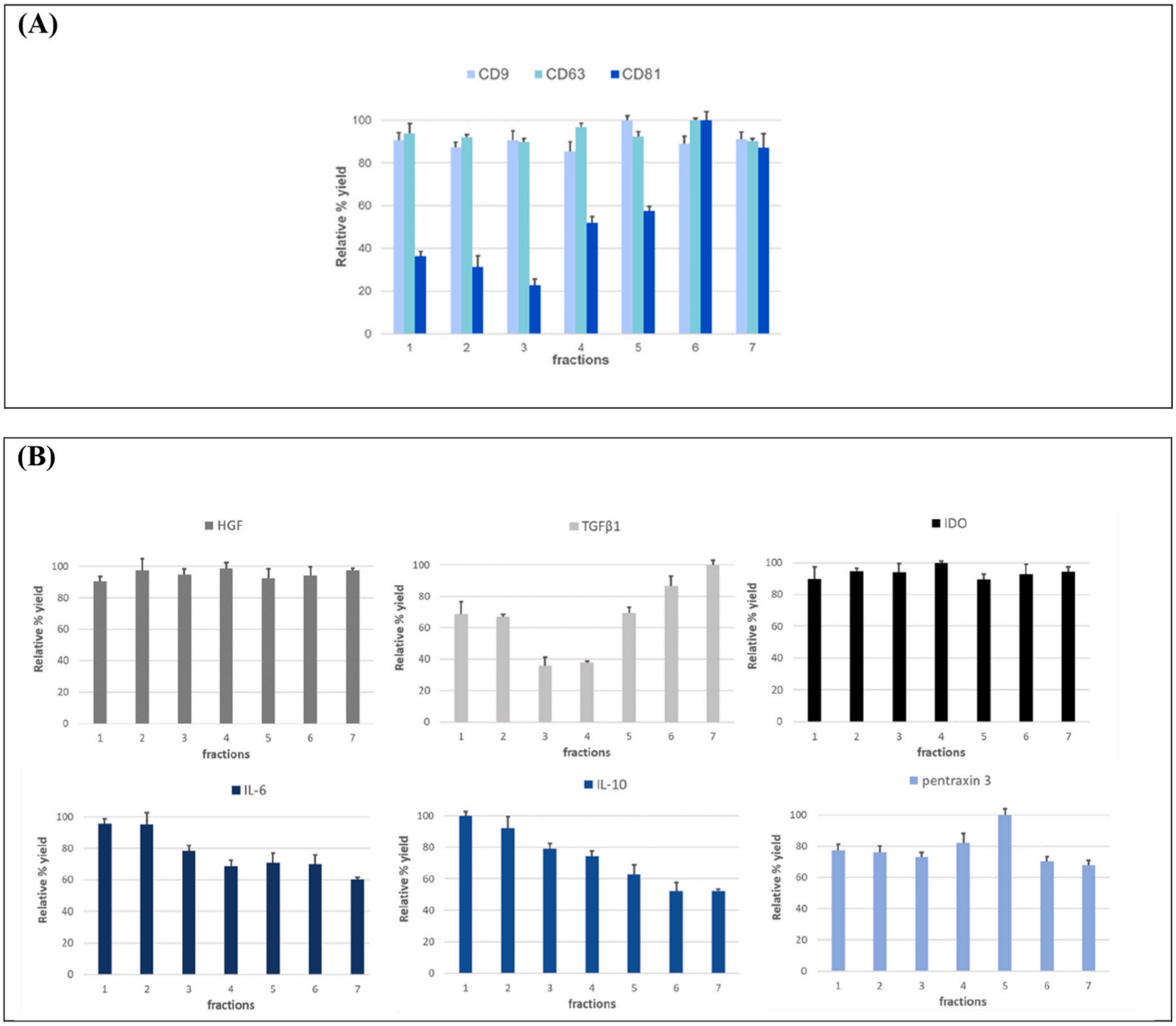

Fig. 3. **(A)** ELISA analysis of EVs fractions for tetraspanins CD9, CD63, and CD81; (B) ELISA analysis of EVs fractions for immunomodulating factors, namely TGFβ1, HGF, IL-10, IDO, IL-6 and pentraxin 3 (N = 3).

pentraxin. On the contrary, IL-10 and IL-6 were less abundant from F3 to F6.

These results confirmed that HF5 can isolate fractions with peculiar properties. However, the uneven distribution of EVs markers and immunomodulating factors highlights the need for a comprehensive characterization to assess secretome identity and purity to make it an efficient product for clinical applications.

3.4. *Proteomic characterization of EVs fractions*

The seven EVs fractions obtained from the hAMSCs secretome and the total EVs fraction were analysed by LC-MS for proteomic analysis (details in Materials and Method section). The combination of top-down and bottom-up approaches as an integrated platform allowed to provide a comprehensive characterization of EVs proteome by investigating either the intact or the enzymatic digested proteomes, respectively, and to complement all results.

The proteomic data have been elaborated by bioinformatic tools to reveal and discuss the different as well as the common features of the EVs fractions analysed, by studying the gene ontology (GO) classification, pathway categories and overrepresentation analysis, considering both shared and exclusive protein elements.. The results obtained are described below in separate paragraphs, based on the proteomic approach used. These results are then compared and finally discussed.

3.4.1. *Bottom-up proteomic analysis of extracellular vesicle fractions*

The raw data obtained by LC-MS analysis of the trypsin digests of the different EVs fractions were elaborated by Proteome Discoverer 1.4 software and filtered according to the Human Proteome Project Mass Spectrometry Data Interpretation Guidelines [54] to ensure high confidence proteins identification. The relative multireport data resulting from elaboration of the duplicate analytical runs of each EVs fraction are reported in Supplementary Table 1S.

Out of the 1038 protein elements totally identified in all EVs fractions analysed, 875 characterized the EVs fractions 1–7, with fraction 4 showing the largest number (Fig. 4A). Grouping analysis disclosed 341 unique proteins out of the 1038 totally identified which included 141 exclusive elements of the different fractions, with fraction 2 and 4 showing their largest number (Fig. 4B).

Two hundred protein elements were instead found in common to all fractions or to part or pair of them (Fig. 4C). It can be observed that fractions 3, 4, 5, 6 and T shared the highest number of proteins, namely, 28 elements, while only 9 proteins were instead common to all fractions.

The lists of proteins identified in each EV fraction have been investigated by STRING tool (highest confidence analysis 0,900) to evidence their possible functional relationships based on gene ontology analysis and classification. The relative networks are depicted in Fig. 5. The networks showed different grade of complexity depending on the EVs fraction and on the number of protein elements within identified. In the networks the red nodes marked the proteins classified as “Extracellular

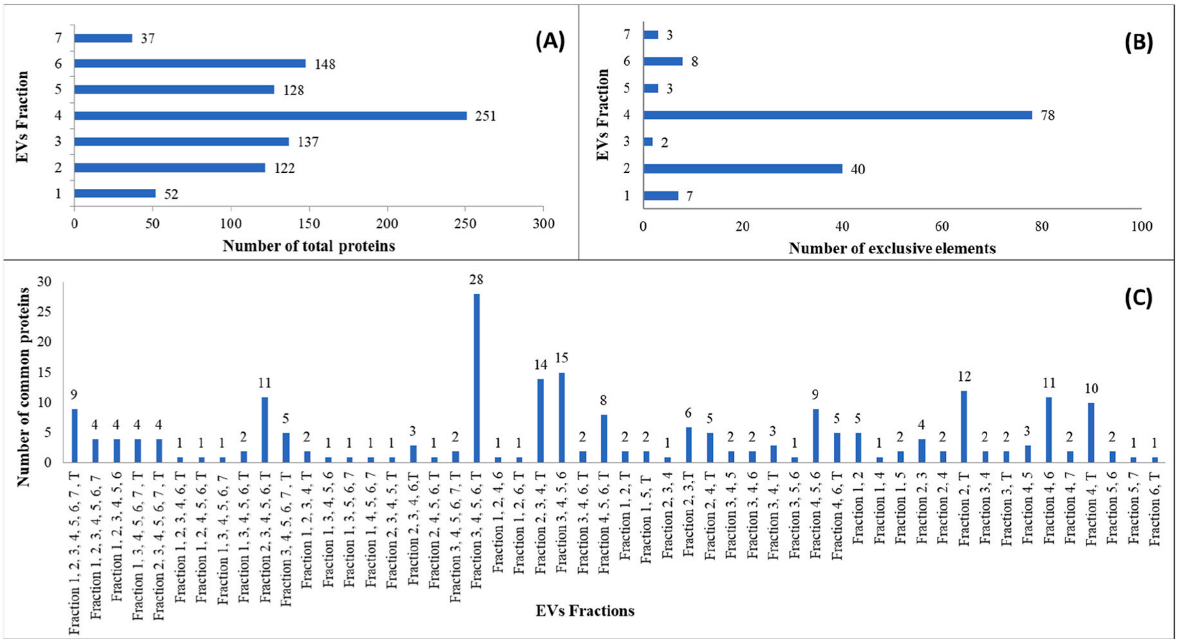

Fig. 4. Number of total (A) exclusive (B) and common (C) protein elements identified in each EVs Fraction.

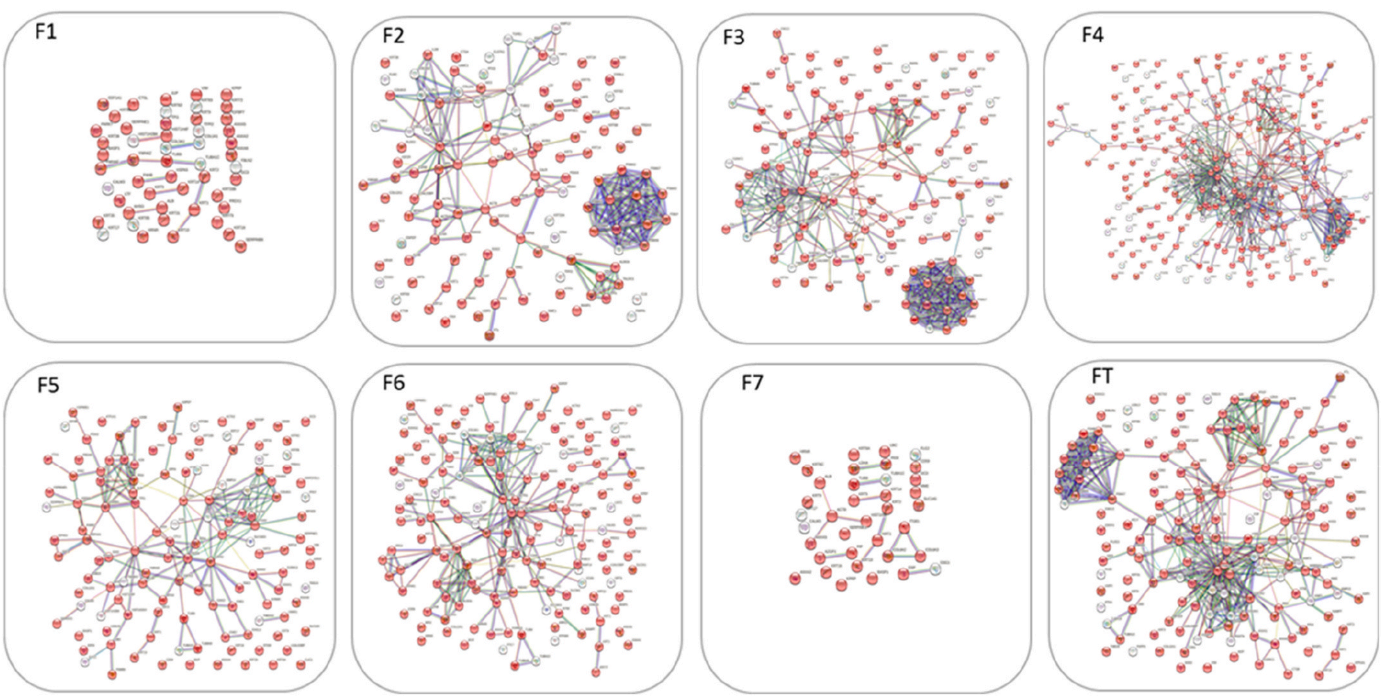

Fig. 5. Functional interaction networks of the total proteins identified in each EVs fraction 1–7 and in the total fraction (FT). The nodes in red marked the extracellular exosomes (EE) classified components.

exosome" (EE) cellular components.

This analysis highlighted different local clusters of interaction significantly enriched in the networks (Supplementary Table 2S). As shown in Fig. 5, fractions F2, F3 and F4 show very similar network profiles in which, on the right side, is evident the crowded cluster of proteasome, playing a key role in the removal of damaged or misfolded proteins by maintaining cellular function and homeostasis. The cluster of "Collagen formation, and Matrix metalloproteinases" (CL:16430) was found significantly enriched in all fractions with the exception of F1 and F7.

F1, F3, F6 and F7 fractions also showed exclusive clusters statistically significantly enriched, namely, CL:36089, CL:16514 and CL:36087 (F1), CL:2688 and CL:2710 (F3), CL:17924 (F6) and CL:16480 (F7) (see Supplementary Table 2S for details).

PANTHER tool analysis of the proteins identified in the different EVs fractions highlighted a different classification of statistically significantly overrepresented pathways (obtained by Fisher's Exact test with Calculate False Discovery Rate correction), as resulting from their grouping analysis (Table 2). With the exception of fractions F4 and F5, all EVs fractions, including FT, did not exhibit exclusive overrepresented

Table 2
Distribution of over-represented pathways in EVs fractions based on grouping analysis of proteomic data elaboration.

Names	Total	Elements
F1 F2 F3 F4 F6 FT	1	Parkinson disease (P00049)
F2 F3 F4 F5 F6 FT	2	Integrin signalling pathway (P00034) Glycolysis (P00024)
F3 F4 F5 F6 FT	5	Huntington disease (P00029) Alzheimer disease-presenilin pathway (P00004) Inflammation mediated by chemokine and cytokine signaling pathway (P00031) Cytoskeletal regulation by Rho GTPase (P00016) Gonadotropin-releasing hormone receptor pathway (P06664)
F3 F4 F5 F6	8	5HT1 type receptor mediated signaling pathway (P04373) Opioid proopiomelanocortin pathway (P05917) Heterotrimeric G-protein signaling pathway-Gi alpha and Gs alpha mediated pathway (P00026) Opioid proenkephalin pathway (P05915) Metabotropic glutamate receptor group II pathway (P00040) Enkephalin release (P05913) Opioid prodynorphin pathway (P05916) Heterotrimeric G-protein signaling pathway-rod outer segment phototransduction (P00028)
F4 F5 F6 FT	1	CCKR signaling map (P06959)
F4 F5 F6	14	PI3 kinase pathway (P00048) Cortocotropin releasing factor receptor signaling pathway (P04380) Muscarinic acetylcholine receptor 2 and 4 signaling pathway (P00043) EGF receptor signaling pathway (P00018) Thyrotropin-releasing hormone receptor signaling pathway (P04394) Oxytocin receptor mediated signaling pathway (P04391) Histamine H2 receptor mediated signaling pathway (P04386) Dopamine receptor mediated signaling pathway (P05912) Histamine H1 receptor mediated signaling pathway (P04385) Beta3 adrenergic receptor signaling pathway (P04379) Heterotrimeric G-protein signaling pathway-Gq alpha and Go alpha mediated pathway (P00027) Angiotensin II-stimulated signaling through G proteins and beta-arrestin (P05911) Muscarinic acetylcholine receptor 1 and 3 signaling pathway (P00042) 5HT4 type receptor mediated signaling pathway (P04376)
F2 FT	1	Pentose phosphate pathway (P02762)
F4 F5	1	5HT2 type receptor mediated signaling pathway (P04374)
F5 F6	5	T cell activation (P00053) Beta1 adrenergic receptor signaling pathway (P04377) Beta2 adrenergic receptor signaling pathway (P04378) Axon guidance mediated by semaphorins (P00007) Nicotinic acetylcholine receptor signaling pathway (P00044)
F4	2	FGF signaling pathway (P00021) Blood coagulation (P00011)
F5	4	Endogenous cannabinoid signaling (P05730) Metabotropic glutamate receptor group III pathway (P00039) Ras Pathway (P04393) Axon guidance mediated by Slit/Robo (P00008)

pathways and almost all shared the statistically significant over-representation of the pathways of Parkinson disease, Integrin signalling and Glycolysis.

Table 3 summarizes the results of the proteomic analysis of the different EVs fractions by comparing the number of the total proteins identified per fraction and the relative Extracellular Exosomes (EE) classified components (number and percent value, third and fourth columns, respectively). In addition, the last two columns report the number of exclusive elements identified per fraction and their gene names, evidencing in bold the relative EE classified elements. In the total

Table 3
Summary of proteomic analysis results of the different EVs fractions.

EVs Fraction (F)	TOT[a] proteins	EE[b] Proteins	EE/TOT % Value	Exclusive proteins of the fraction n. (n. EE)[c]	Gene name exclusive proteins (EE)[c]
F1	52	40	76.0 %	7 (**5**)	HSP77, FBLN2, **SERPINB6, PARK7, IGFBP7, CTSL, KRT72**
F2	122	92	75.4 %	40 (**23**)	FLNC, CO5A2, C1S, TIMP2, CSTN1, PSAL, CBPA4, KT33A, POSTN, PDIA4, PTX3, MMP2, MMP10, AXA2L, SPRC, C163A, FBN2, **LAP3, CAT, C3, CHI3L1, GNS, ATRN, LUM, APEH, COL1A2, GAA, CALR, TALDO1, NME1, CTSB, IGF2R, ITIH2, CTSA, SPTAN1, FAH, TKT, GPI, FLNB, SOD2**
F3	137	112	81.7 %	2 (**0**)	CO5A1, APOB
F4	251	208	82.9 %	78 (**61**)	ERLN2, MPZL1, RPN1, RAP2A, TF, LAMA2, CTNA1, TBA1B, GALT2, STAM1, RAB1C, CDCP1, APMAP, FPRP, RAB23, TMED7, FARP1, **ACTR2, AHCY, ANXA3, ANXA7, ARF3, ARHGDIA, BST1, CCT2, CCT3, CCT8, CLIC4, CNP, CPNE3, CTNND1, EHD1, EHD2, EHD4, FLOT1, GNAQ, GNAS, GNB2L1, GSTP1, HBA2, HBB, HGS, HLA-A, HLA-B, HSP90AA1, HSPA6, ITGA3, ITGB3, LMAN2, MYOF, NRAS, PCYOX1, PDCD6, PDCD6IP, PFKP, PHGDH, PLOD1, PLXNB2, PPIB, RAB11A, RAB13, RAC1, RALA, RAP1A, RNH1, RPS8, SCARB2, SLC16A1, SLC44A1, SLC44A2, SLC7A5, SSR4, THY1, TM9SF2, TXN, WDR1, YWHAG, YWHAQ**
F5	128	108	84.4 %	3 (**0**)	KRT86, K1C13, TYB4
F6	148	126	85.1 %	8 (**6**)	OST48, NDK8, **LEG7, K2C79, K2C1B, TCTP, 6PGD, RS2**

(*continued on next page*)

Table 3 (*continued*)

EVs Fraction (F)	TOT[a] proteins	EE[b] Proteins	EE/ TOT % Value	Exclusive proteins of the fraction n. (n. EE)[c]	Gene name exclusive proteins (EE)[c]
F7	37	32	86.5 %	3 (**0**)	PIP, ZA2G, DSG1
FT	163	134	82.2 %	–	–

[a] after filtering data for high confidence, details in materials and method section.
[b] EE, Extracellular Exosomes components classified proteins.
[c] in bold the EE proteins exclusive of each fraction.

fraction (FT), 134 proteins out of the 163 totally identified were classified as EE proteins, i.e., the 82.2 %. It is noteworthy that the number of EE classified proteins increases from EV fraction 1 to 7, reaching the 86.5 % of the total proteins in fraction 7.

The list of the exclusive proteins identified in each EVs fraction is reported in Supplementary Table 3S. The EVs fractions F1, F2, F4 and F6, showed a fair number of exclusive proteins moreover containing an high percent value of EE elements with predicted relationships, especially for F4 and F2, as resulting from functional network analysis by STRING tool (Fig. 1S, EE protein nodes in red). In the specific networks of F2 and F4 fractions, selected molecular functions resulted statistically significantly enriched (Table 4S).

Relative to fractions F2 and F4, showing the highest number of exclusive proteins, we further investigate with the Reactome tool the relative classification in the pathways of Immune System, Developmental biology, Extracellular matrix organization, Homeostasis and Cellular response, connected to the relevant biological activities exerted by the hAMSCs secretome (results in Tables 4 and 5). Several exclusive proteins of EVs fractions F2 and F4 are classified in these pathways , with a prevalence of Immune System for F2.

3.4.2. *Top-down proteomic analysis of extracellular vesicle fractions*

The fraction below 10 kDa resulting from FASP filtration of each EVs fractions F1-7 and FT was collected and submitted to duplicate LC-MS

Table 4
Classification of the exclusive proteins identified in EVs fraction F2 inside the pathways of Immune System, Developmental biology, Extracellular matrix organization, Homeostasis and Cellular response[a].

Gene name	40 Exclusive proteins (EE)** Fraction 2	Uniprot Accession	Immune System	Developmental biology	Extracellular matrix organization	Hemostasis	Cellular responce to stimoli
ACPH	**Acylamino-acid-releasing enzyme**	**P13798**	●				
ATRN	**Attractin**	**O75882**					
CALR	**Calreticulin**	**P27797**	●				●
CATA	**Catalase**	**P04040**	●				●
CATB	**Cathepsin B**	**P07858**	●		●		
MPRI	**Cation-independent mannose-6-phosphate receptor**	**P11717**	●				
CH3L1	**Chitinase-3-like protein 1**	**P36222**	●				
CO1A2	**Collagen alpha-2(I) chain**	**P08123**	●		●	●	
CO3	**Complement C3**	**P01024**	●				
AMPL	**Cytosol aminopeptidase**	**P28838**					
FLNB	**Filamin-B**	**O75369**	●				
FAAA	**Fumarylacetoacetase**	**P16930**					
G6PI	**Glucose-6-phosphate isomerase**	**P06744**	●				
ITIH2	**Inter-alpha-trypsin inhibitor heavy chain H2**	**P19823**					
LUM	**Lumican**	**P51884**			●		
LYAG	**Lysosomal alpha-glucosidase**	**P10253**	●				
PPGB	**Lysosomal protective protein**	**P10619**	●				
GNS	**N-acetylglucosamine-6-sulfatase**	**P15586**	●				
NDKA	**Nucleoside diphosphate kinase A**	**P15531**					
SPTN1	**Spectrin alpha chain, non-erythrocytic 1**	**Q13813**	●	●			
SODM	**Superoxide dismutase [Mn], mitochondrial**	**P04179**	●				●
TALDO	**Transaldolase**	**P37837**	●				●
TKT	**Transketolase**	**P29401**					●
MMP2	72 kDa type IV collagenase	P08253	●	●	●		
CSTN1	Calsyntenin-1	O94985					
CBPA4	Carboxypeptidase A4	Q9UI42					
CO5A2	Collagen alpha-2(V) chain	P05997		●	●		
C1S	Complement C1s subcomponent	P09871	●				
FBN2	Fibrillin-2	P35556			●		
FLNC	Filamin-C	Q14315					
KT33A	Keratin, type I cuticular Ha3-I	O76009		●			
TIMP2	Metalloproteinase inhibitor 2	P16035	●		●		
PTX3	Pentraxin-related protein PTX3	P26022	●				
POSTN	Periostin	Q15063					
PDIA4	Protein disulfide-isomerase A4	P13667					
PSAL	Puromycin-sensitive aminopeptidase-like protein	A6NEC2					
AXA2L	Putative annexin A2-like protein	A6NMY6					
C163A	Scavenger receptor cysteine-rich type 1 protein M130	Q86VB7					
SPRC	SPARC	P09486			●	●	
MMP10	Stromelysin-2	P09238			●		

**in bold the EE exclusive proteins.
[a] based on Reactome proteins pathways classification.

Table 5
Classification of the exclusive proteins identified in EVs fraction F4 inside the pathways of Immune System, Developmental biology, Extracellular matrix organization, Homeostasis and Cellular response[a].

Gene name	78 Exclusive proteins (EE)**Fraction 4	Uniprot Accession	Immune System	Developmental biology	Extracellular matrix organization	Hemostasis	Cellular responce to stimoli
1433G	**14-3-3 protein gamma**	**P61981**					
1433T	**14-3-3 protein theta**	**P27348**					
CN37	**2′,3′-cyclic-nucleotide 3′-phosphodiesterase**	**P09543**					
RS8	**40S ribosomal protein S8**	**P62241**		●			●
ARP2	**Actin-related protein 2**	**P61160**	●	●			
SAHH	**Adenosylhomocysteinase**	**P23526**					
BST1	**ADP-ribosyl cyclase/cyclic ADP-ribose hydrolase 2**	**Q10588**	●				
ARF3	**ADP-ribosylation factor 3**	**P61204**					
ANXA3	**Annexin A3**	**P12429**					
ANXA7	**Annexin A7**	**P20073**					
PFKAP	**ATP-dependent 6-phosphofructokinase, platelet type**	**Q01813**					
CTND1	**Catenin delta-1**	**O60716**					
CLIC4	**Chloride intracellular channel protein 4**	**Q9Y696**					
CTL1	**Choline transporter-like protein 1**	**Q8WWI5**					
CTL2	**Choline transporter-like protein 2**	**Q8IWA5**	●				
CPNE3	**Copine-3**	**O75131**	●				
SERA	**D-3-phosphoglycerate dehydrogenase**	**O43175**					
EHD1	**EH domain-containing protein 1**	**Q9H4M9**				●	
EHD2	**EH domain-containing protein 2**	**Q9NZN4**				●	
EHD4	**EH domain-containing protein 4**	**Q9H223**					
FLOT1	**Flotillin-1**	**O75955**					
GSTP1	**Glutathione S-transferase P**	**P09211**	●				●
RASN	**GTPase NRas**	**P01111**	●	●		●	
GNAQ	**Guanine nucleotide-binding protein G(q) subunit alpha**	**P50148**				●	
GNAS2	**Guanine nucleotide-binding protein G(s) subunit alpha isoforms short**	**P63092**				●	
HSP76	**Heat shock 70 kDa protein 6**	**P17066**	●				●
HS90A	**Heat shock protein HSP 90-alpha**	**P07900**	●	●			●
HBA	**Hemoglobin subunit alpha**	**P69905**					●
HBB	**Hemoglobin subunit beta**	**P68871**	●			●	●
HGS	**Hepatocyte growth factor-regulated tyrosine kinase substrate**	**O14964**					
HLAA	**HLA class I histocompatibility antigen, A alpha chain**	**P04439**	●				
HLAB	**HLA class I histocompatibility antigen, B alpha chain**	**P01889**	●				
ITA3	**Integrin alpha-3**	**P26006**			●	●	
ITB3	**Integrin beta-3**	**P05106**		●	●	●	
LAT1	**Large neutral amino acids transporter small subunit 1**	**Q01650**				●	
SCRB2	**Lysosome membrane protein 2**	**Q14108**					
MOT1	**Monocarboxylate transporter 1**	**P53985**				●	
MYOF	**Myoferlin**	**Q9NZM1**					
PPIB	**Peptidyl-prolyl cis-trans isomerase B**	**P23284**			●		
PLXB2	**Plexin-B2**	**O15031**					
PCYOX	**Prenylcysteine oxidase 1**	**Q9UHG3**					
PLOD1	**Procollagen-lysine,2-oxoglutarate 5-dioxygenase 1**	**Q02809**			●		
PDC6I	**Programmed cell death 6-interacting protein**	**Q8WUM4**					
PDCD6	**Programmed cell death protein 6**	**O75340**					
RAC1	**Ras-related C3 botulinum toxin substrate 1**	**P63000**	●	●		●	
RB11A	**Ras-related protein Rab-11A**	**P62491**					
RAB13	**Ras-related protein Rab-13**	**P51153**					
RALA	**Ras-related protein Ral-A**	**P11233**	●				
RAP1A	**Ras-related protein Rap-1A**	**P62834**	●			●	
RACK1	**Receptor of activated protein C kinase 1**	**P63244**					
GDIR1	**Rho GDP-dissociation inhibitor 1**	**P52565**					
RINI	**Ribonuclease inhibitor**	**P13489**					
TCPB	**T-complex protein 1 subunit beta**	**P78371**	●				
TCPG	**T-complex protein 1 subunit gamma**	**P49368**					
TCPQ	**T-complex protein 1 subunit theta**	**P50990**	●				
THIO	**Thioredoxin**	**P10599**	●				●
THY1	**Thy-1 membrane glycoprotein**	**P04216**					
SSRD	**Translocon-associated protein subunit delta**	**P51571**					
TM9S2	**Transmembrane 9 superfamily member 2**	**Q99805**					
LMAN2	**Vesicular integral-membrane protein VIP36**	**Q12907**					
WDR1	**WD repeat-containing protein 1**	**O75083**				●	
APMAP	Adipocyte plasma membrane-associated protein	Q9HDC9					

(*continued on next page*)

Table 5 (*continued*)

Gene name	78 Exclusive proteins (EE)**Fraction 4	Uniprot Accession	Immune System	Developmental biology	Extracellular matrix organization	Hemostasis	Cellular responce to stimoli
CTNA1	Catenin alpha-1	P35221		●			
CDCP1	CUB domain-containing protein 1	Q9H5V8					
RPN1	Dolichyl-diphosphooligosaccharide–protein glycosyltransferase subunit 1	P04843					
ERLN2	Erlin-2	O94905					
FARP1	FERM, ARHGEF and pleckstrin domain-containing protein 1	Q9Y4F1					
LAMA2	Laminin subunit alpha-2	P24043		●	●		
MPZL1	Myelin protein zero-like protein 1	O95297					
GALT2	Polypeptide N-acetylgalactosaminyltransferase 2	Q10471					
FPRP	Prostaglandin F2 receptor negative regulator	Q9P2B2					
RAB1C	Putative Ras-related protein Rab-1C	Q92928					
RAB23	Ras-related protein Rab-23	Q9ULC3					
RAP2A	Ras-related protein Rap-2a	P10114					
STAM1	Signal transducing adapter molecule 1	Q92783					
TF	Tissue factor	P13726				●	
TMED7	Transmembrane emp24 domain-containing protein 7	Q9Y3B3					
TBA1B	Tubulin alpha-1B chain	P68363	●	●		●	●

**in bold the EE exclusive proteins.
[a] based on Reactome proteins pathways classification.

proteomic analysis following the top-down approach after a protein precipitation protocol (see Material and Method section for details). Differently from the bottom-up approach, the top-down strategy aims to characterize small proteins and peptides in their intact forms. The strategy is challenging for studying the naturally occurring protein fragments and the cryptides, i.e. peptide fragments from major proteins with proper biological activity [62], and to characterize isoforms and post-translational modifications (PTMs).

The analysis identified a total of 72 uniprot accessions in all EVs fractions analysed, each identified by one or more relative peptide fragments. No intact proteins (100 % sequence coverage) were identified in the <10 kDa fraction analysed. Out of the 72 uniprot accessions, 48 were identified F1-F7, while 24 in the FT (complete top-down identification data are in Supplementary Table 5S). The group of 48 proteins included 33 uniprot accessions which exclusively characterized the different EVs fractions (Fig. 6), as resulting from grouping analysis.

Table 6 reports the list of the peptides identified in EVs fractions with the reference of the relative parent protein. Proteins and peptides with unmeasurable area in the LC-MS replicate, as resulting from Proteome Discoverer 1.4 LC-MS data elaboration, were excluded from elaboration.

Noteworthy, the identification in almost all EVs fractions of the peptide PFIAIHAESKL (MH+ 1225.70 Da) corresponding to the C-terminal fragment 501–511 of the Pancreatic alpha-amylase, and of the peptide GEYKFQNALLVR (MH^+ 1479.80 Da) corresponding to fragment 423–434 of Albumin and carrying the N-terminal acetylation post-translation modification (PTM). These peptides were undetected in the total fraction FT.

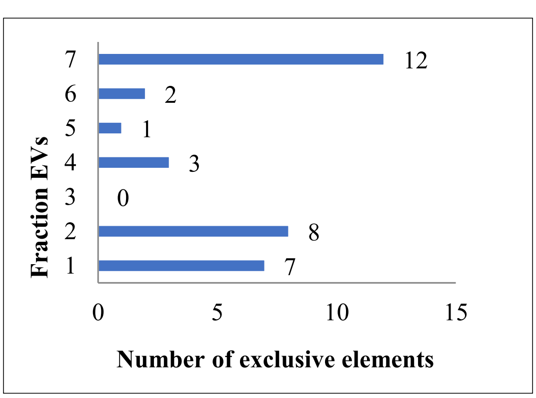

Fig. 6. Number of exclusive elements of the different EVs Fractions analysed by Top-down approach.

The Pancreatic alpha-amylase peptide fragment with sequence PFIAIHAESKL was predicted for antimicrobial activity [63]. Concerning Albumin, it is well known that the protein is a source of bioactive peptide fragments that leave the cell by exocytosis [64]. Particularly, the albumin peptide identified in the present investigation contains the sequence FQNAL, a pentapeptide named Cabin-A2, reported as an inhibitor of cathepsin B [65] and anti-cathepsin B drug candidate [66]. According to the concept of cryptides [62], the fragment peptides identified, some of them carrying N-terminal acetylation or methionine oxidation PTMs, could disclose proper biological activities, contributing to specific properties of the hAMSCs secretome, as well as they could simply represent the phenotypic manifestation of proteases activities.

Consistent with the anti-inflammatory properties of hAMSCs secretome, it is interesting to remark that the proteins in Table 6 are mapped to contain predicted anti-inflammatory epitopes in their full sequence, according to the Antiinflam tool (http://metagenomics.iiserb.ac.in/antiinflam/search.php) [67], and that some of the identified peptide fragments of these proteins are included, totally or in part, in these sequence traits(Table 6). Among them is included the fragment 20–40 of thymosin beta 4, the main G-actin sequestering peptide, that interestingly includes part of the sequence trait 17–23 LKKTETQ, reported for to be associated to actin binding, promotion of hair growth, improvement of dermal wound healing, angiogenesis stimulation and mast cell exocytosis induction [68].

4. Conclusions

In this study, for the first time we employed a low-volume FFF separation technique to analyze the hAMSC secretome, specifically targeting the extracellular vesicle (EV) component. This approach enabled the fractionation of EVs and thereby unveil new insights into the fraction-specific properties of EVs, including their size, cargo content, and functions. Particularly, we developed and introduced a novel method capable of isolating and characterizing homogeneous EV fractions in their natural state from the conditioned medium of hAMSCs. The outcomes of this study have shown that the different EV fractions possess varying biological capabilities, a diversity that can be attributed to the detailed proteomic characterization supplemented by ELISA assays.

Specifically, the two different proteomic approaches applied, namely the bottom-up, based on FASP digestion, and the top-down,

Table 6
Top-down identification data of EVs fraction 1–7 and FT: Uniprot accession and protein name, identified peptide fragments with relative modifications and monoisotopic molecular mass value.

Accession	Protein Description	Σ Coverage	Fragment	Peptide Sequence	Modifications	MH + [Da]
F1						
P02768	Albumin	1.97	**423–434**	**GEYKFQNALLVR**	N-Term(Acetyl)	1479.80144
P04264	Keratin, type II cytoskeletal 1	1.40	**501–509**	VSVSVSTSH		902.45897
P04746	Pancreatic alpha-amylase	2.15	**501–511**	**PFIAIHAESKL**		1225.69727
F2						
P00403	Cytochrome *c* oxidase subunit 2	4.41	**28–37**	LMIIFLICFL		1225.70304
O60264	SWI/SNF-related matrix-associated actin-dependent regulator of chromatin subfamily A member 5	2.57	**589–615**	AMDRAHRIGQTKTVRVFRFITDNTVEE	M2(Oxidation)	3206.65388
O60683	Peroxisome biogenesis factor 10	2.45	**158–165**	RALLRAVF	N-Term(Acetyl)	987.60289
P04746	Pancreatic alpha-amylase	2.15	**501–511**	**PFIAIHAESKL**		1225.70066
P02768	Albumin	1.97	**423–434**	**GEYKFQNALLVR**	N-Term(Acetyl)	1479.80852
F3						
P04746	Pancreatic alpha-amylase	2.15	**501–511**	**PFIAIHAESKL**		1225.70084
P02768	Albumin	1.97	**423–434**	**GEYKFQNALLVR**	N-Term(Acetyl)	1479.80486
F4						
Q68BL7	Olfactomedin-like protein 2A	5.06	**208–240**	AAAPATPATGTGSKAQDTARGKGKDISKYGSVQ		3190.64809
Q9H6T3	RNA polymerase II-associated protein 3	4.06	**269–295**	ERKQIEAQQNKQQAISEKDRGNGFFKE		3206.63862
P04746	Pancreatic alpha-amylase	2.15	**501–511**	**PFIAIHAESKL**		1225.69791
P02768	Albumin	1.97	**423–434**	**GEYKFQNALLVR**	N-Term(Acetyl)	1479.80449
F5						
P02768	Albumin	1.97	**423–434**	**GEYKFQNALLVR**	N-Term(Acetyl)	1479.80657
F6						
P04746	Pancreatic alpha-amylase	2.15	**501–511**	**PFIAIHAESKL**		1225.70221
P02768	Albumin	1.97	**423–434**	**GEYKFQNALLVR**	N-Term(Acetyl)	1479.80742
F7						
A6NIR3	Arf-GAP with GTPase, ANK repeat and PH domain-containing protein 5	8.45	**450–507**	ESSKSKSQLTSQSEAMALQSIQNMRGNAHCVDYETQNPKWASLNLGVLMCIECSGIHR	M24(Oxidation); M49 (Oxidation)	6441.03196
P63261	Actin, cytoplasmic 2	3.20	**2–13**	EEEIAALVIDNG	N-Term(Acetyl)	1314.64751
P0CG39	POTE ankyrin domain family member J	2.22	**879–901**	LCYVALDFEQEMAMVASSSSLEK		2551.17698
P04746	Pancreatic alpha-amylase	2.15	**501–511**	**PFIAIHAESKL**		1225.69672
FT						
P62328	Thymosin beta-4	56.82	**20–40**	KTETQEKNPLPSKETIEQEKQ		2485.29897
P80723	Brain acid soluble protein 1	48.02	**164–184**	SDGAPASDSKPGSSEAAPSSK		1932.89316
			39–52	ESEPQAAAEPAEAK		1427.67644
			80–97	EEAPKAEPEKTEGAAEAK		1884.93509
			21–38	EKDKKAEGAATEEEGTPK		1917.95742
			185–198	ETPAATEAPSSTPK		1386.68523
			26–52	AEGAATEEEGTPKESEPQAAAEPAEAK		2698.25699
P05204	Non-histone chromosomal protein HMG-17	42.22	**12–24**	GDKAKVKDEPQRR		1526.84975
			30–46	AKPAPPKPEPKPKKAPA		1752.06785
			5–18	KAEGDAKGDKAKVK		1444.82058
O60814	Histone H2B type 1-K	27.78	**2–21**	PEPAKSAPAPKKGSKKAVTK		2020.20795
P10412	Histone H1.4	17.81	**2–26**	SETAPAAPAAPAPAEKTPVKKKARK	N-Term(Acetyl)	2557.46839
			2–23	SETAPAAPAAPAPAEKTPVKKK	N-Term(Acetyl)	2202.23012
			2–25	SETAPAAPAAPAPAEKTPVKKKAR	N-Term(Acetyl)	2429.36704
			33–46	RKASGPPVSELITK		1482.87806
			6–26	PAAPAAPAPAEKTPVKKKARK		2127.29702
			6–25	PAAPAAPAPAEKTPVKKKAR		1999.19533
P62805	Histone H4	13.59	**24–37**	RDNIQGITKPAIRR		1637.96377
P29966	Myristoylated alanine-rich C-kinase substrate	9.94	**138–153**	AEDGATPSPSNETPKK		1628.78647
			138–152	AEDGATPSPSNETPK		1500.69499
			177–193	EAGEGGEAEAPAAEGGK		1529.68425
P25788	Proteasome subunit alpha type-3	5.49	**242–255**	ESLKEEDESDDDNM	M14(Oxidation)	1671.63140
Q8NC51	Plasminogen activator inhibitor 1 RNA-binding protein	5.15	**32–52**	KAAENKKKEAGGGGVGGPGAK		1911.05361
Q5T4B2	Inactive glycosyltransferase 25 family member 3	4.20	**443–467**	LIYLGRKQVNPEKETAVEGLPGLVV	N-Term(Acetyl)	2764.58512
Q6NSW5	Putative DENN domain-containing protein 10 B	3.64	**136–148**	QSEENGSFLSKDF	N-Term(Acetyl)	1529.68877
P68363	Tubulin alpha-1B chain	2.66	**440–451**	VEGEGEEEGEEY		1355.52434
Q9HC36	rRNA methyltransferase 3, mitochondrial	2.38	**12–21**	VRPLLQVVQA	N-Term(Acetyl)	1164.72099
P21709	Ephrin type-A receptor 1	1.02	**792–801**	WTAPEAIAHR	N-Term(Acetyl)	1193.61032
P12111	Collagen alpha-3(VI) chain	0.41	**1348–1360**	SDDEVDDPAVELK		1431.66155

investigating the intact small proteins and peptides, provided a comprehensive characterization of the EVS fractions proteome in a large range of molecular mass. The EVs fractions showed different proteomic profiles, with fraction 2 and 4 exhibiting the largest number of exclusive elements. Gene ontology analysis revealed the cluster of "Collagen formation, and Matrix metalloproteinases" as enriched in almost all EVs fractions and the increase of the % value of EE proteins over the total identified from fraction 1 to 7. Interestingly about the 67 % and 43 % of the exclusive proteins of fractions F2 and F4 were classified as involved in the pathways of Immune System, Developmental biology, Extracellular matrix organization, Homeostasis and Cellular response, most likely depicting the relevant hAMSCs secretome biological activities. Furthermore, top-down proteomic analysis consistently identified two small peptide fragments from Albumin and Pancreatic alpha-amylase across all EV fractions, suggesting roles that warrant further exploration. Additionally, analyses with ELISA revealed variations in key biological modulators such as IL-6, IL-10, and TGF-beta, which could imply possible significant changes in the therapeutic action of different vesicular fractions. These results indicate that HF5 allowed to identify fractions particularly enriched in proteins that could be of greater functional interest. The presented method indeed highlights the existence of differences not only in size/physical parameters and marker expression, but also in proteomic composition among the different vesicular fractions isolated from the hAMSC secretome, that can support functional differences thus suggesting different therapeutic applications.

CRediT authorship contribution statement

Valentina Marassi: Writing – review & editing, Visualization, Investigation, Conceptualization. **Giampiero La Rocca:** Writing – review & editing, Writing – original draft, Funding acquisition, Formal analysis, Data curation, Conceptualization. **Anna Placci:** Writing – review & editing, Methodology, Investigation. **Alexandra Muntiu:** Writing – review & editing, Methodology, Investigation. **Federica Vincenzoni:** Writing – review & editing, Methodology. **Alberto Vitali:** Writing – review & editing, Methodology. **Claudia Desiderio:** Writing – review & editing, Writing – original draft, Methodology, Data curation, Conceptualization. **Tullia Maraldi:** Writing – review & editing, Writing – original draft, Formal analysis. **Francesca Beretti:** Writing – original draft, Methodology, Formal analysis. **Eleonora Russo:** Writing – review & editing, Formal analysis, Data curation. **Vitale Miceli:** Writing – review & editing, Formal analysis, Data curation. **Pier Giulio Conaldi:** Writing – review & editing, Formal analysis, Data curation. **Andrea Papait:** Writing – review & editing, Formal analysis, Data curation. **Pietro Romele:** Writing – review & editing, Writing – original draft, Data curation, Conceptualization. **Anna Cargnoni:** Writing – review & editing, Writing – original draft, Data curation, Conceptualization. **Antonietta Rosa Silini:** Writing – review & editing, Writing – original draft, Formal analysis, Data curation, Conceptualization. **Francesco Alviano:** Writing – review & editing, Writing – original draft, Methodology, Conceptualization. **Ornella Parolini:** Writing – review & editing, Writing – original draft, Funding acquisition, Formal analysis, Data curation, Conceptualization. **Stefano Giordani:** Writing – review & editing, Methodology, Formal analysis. **Andrea Zattoni:** Writing – review & editing, Resources, Investigation. **Pierluigi Reschiglian:** Writing – review & editing, Resources, Conceptualization. **Barbara Roda:** Writing – review & editing, Visualization, Supervision, Conceptualization.

Funding

The authors declare that they have no known competing financial interests or personal relationships that could have appeared to influence the work reported in this paper: Ornella Parolini reports financial support was provided by PRIN 2017 program of Italian Ministry of Research and University (MIUR, Grant No. 2017RSAFK7). If there are other authors, they declare that they have no known competing financial interests or personal relationships that could have appeared to influence the work reported in this paper.

Data availability

Data will be made available on request.

Acknowledgements

This research was funded by PRIN 2017 program of Italian Ministry of Research and University (MIUR, Grant No. 2017RSAFK7)

Appendix A. Supplementary data

Supplementary data to this article can be found online at https://doi.org/10.1016/j.talanta.2024.126216.

References

[1] A.R. Silini, M. Magatti, A. Cargnoni, O. Parolini, Is immune modulation the mechanism underlying the beneficial effects of amniotic cells and their derivatives in regenerative medicine? Cell Transplant. 26 (2017) 531–539.
[2] M. Krampera, K. Le Blanc, Mesenchymal stromal cells: putative microenvironmental modulators become cell therapy, Cell Stem Cell 28 (2021) 1708–1725.
[3] V. Miceli, et al., Different priming strategies improve distinct therapeutic capabilities of mesenchymal stromal/stem cells: potential implications for their clinical use, World J. Stem Cell. 15 (2023) 400.
[4] D. Rossi, S. Pianta, M. Magatti, P. Sedlmayr, O. Parolini, Characterization of the conditioned medium from amniotic membrane cells: prostaglandins as key effectors of its immunomodulatory activity, PLoS One 7 (2012) e46956.
[5] M.F. Pittenger, D.E. Discher, B.M. Péault, D.G. Phinney, Mesenchymal Stem Cell Perspective: Cell Biology to Clinical Progress, vol. 4, 2019, p. 22.
[6] V. Miceli, et al., Therapeutic properties of mesenchymal stromal/stem cells: the need of cell priming for cell-free therapies in regenerative medicine, Int. J. Mol. Sci. 22 (2021) 763.
[7] M. Kou, et al., Mesenchymal stem cell-derived extracellular vesicles for immunomodulation and regeneration: a next generation therapeutic tool? Cell Death Dis. 13 (2022) 580.
[8] D. D'Arrigo, et al., Secretome and extracellular vesicles as new biological therapies for knee osteoarthritis: a systematic review, J. Clin. Med. (2019), https://doi.org/10.3390/jcm8111867.
[9] S. Keshtkar, N. Azarpira, M.H. Ghahremani, Mesenchymal stem cell-derived extracellular vesicles: novel frontiers in regenerative medicine, Stem Cell Res. Ther. 9 (2018) 63.
[10] A. Cargnoni, et al., Conditioned medium from amniotic membrane-derived cells prevents lung fibrosis and preserves blood gas exchanges in bleomycin-injured mice-specificity of the effects and insights into possible mechanisms, Cytotherapy 16 (2014) 17–32.
[11] C. Giampà, et al., Conditioned medium from amniotic cells protects striatal degeneration and ameliorates motor deficits in the R6/2 mouse model of Huntington's disease, J. Cell Mol. Med. 23 (2019) 1581–1592.
[12] F. Pischiutta, et al., Protection of brain injury by amniotic mesenchymal stromal cell-secreted metabolites, Crit. Care Med. 44 (2016) e1118–e1131.
[13] S. Pianta, et al., Amniotic membrane mesenchymal cells-derived factors skew T cell polarization toward Treg and downregulate Th1 and Th17 cells subsets, Stem Cell Rev. 11 (2015) 394–407.
[14] A. Papait, et al., Comparison of EV-free fraction, EVs, and total secretome of amniotic mesenchymal stromal cells for their immunomodulatory potential: a translational perspective, Front. Immunol. 13 (2022) 960909.
[15] A.R. Silini, et al., CM from Intact hAM: an Easily Obtained Product with Relevant Implications for Translation in Regenerative Medicine, vol. 12, 2021, p. 540.
[16] M. Magatti, et al., Human amnion favours tissue repair by inducing the M1-to-M2 switch and enhancing M2 macrophage features, Journal of tissue engineering and regenerative medicine 10 (2016) 2895–2911.
[17] M. Bulati, et al., The immunomodulatory properties of the human amnion-derived mesenchymal stromal/stem cells are induced by INF-γ produced by activated lymphomonocytes and are mediated by cell-to-cell contact and soluble factors, Front. Immunol. 11 (2020) 54.
[18] E. Ragni, A. Papait, C. Perucca Orfei, Amniotic Membrane-Mesenchymal Stromal Cells Secreted Factors and Extracellular Vesicle-miRNAs: Anti-inflammatory and Regenerative Features for Musculoskeletal Tissues, 2021.
[19] M. Bulati, et al., 3D culture and interferon-γ priming modulates characteristics of mesenchymal stromal/stem cells by modifying the expression of both intracellular and exosomal microRNAs, Biology 12 (2023) 1063.
[20] E. Munoz-Perez, A. Gonzalez-Pujana, M. Igartua, E. Santos-Vizcaino, R. M. Hernandez, Mesenchymal stromal cell secretome for the treatment of immune-mediated inflammatory diseases: latest trends in isolation, content optimization and delivery avenues, Pharmaceutics 13 (2021) 1802.

[21] K.-A. Cho, M. Park, Y.-H. Kim, S.-Y. Woo, K.-H. Ryu, RNA sequencing reveals a transcriptomic portrait of human mesenchymal stem cells from bone marrow, adipose tissue, and palatine tonsils, Sci. Rep. 7 (2017) 17114.
[22] J. Woo, D. Han, J. Park, S.J. Kim, Y. Kim, In-depth characterization of the secretome of mouse CNS cell lines by LC-MS/MS without prefractionation, Proteomics 15 (2015) 3617–3622.
[23] N.K. Dubey, et al., Revisiting the advances in isolation, characterization and secretome of adipose-derived stromal/stem cells, Int. J. Mol. Sci. 19 (2018) 2200.
[24] A. Gallo, et al., Changes in the transcriptome profiles of human amnion-derived mesenchymal stromal/stem cells induced by three-dimensional culture: a potential priming strategy to improve their properties, Int. J. Mol. Sci. 23 (2022) 863.
[25] G. Vergauwen, et al., Robust sequential biophysical fractionation of blood plasma to study variations in the biomolecular landscape of systemically circulating extracellular vesicles across clinical conditions, J. Extracell. Vesicles 10 (2021) e12122.
[26] L.M. Doyle, M.Z. Wang, Overview of extracellular vesicles, their origin, composition, purpose, and methods for exosome isolation and analysis, Cells 8 (2019) 727.
[27] J. Wankar, et al., Widening the therapeutic perspectives of clofazimine by its loading in sulfobutylether β-cyclodextrin nanocarriers: nanomolar IC 50 values against MDR S. Epidermidis, Mol. Pharm. 15 (2018) 3823–3836.
[28] J.S. Yang, J.Y. Kim, J.C. Lee, M.H. Moon, Investigation of lipidomic perturbations in oxidatively stressed subcellular organelles and exosomes by asymmetrical flow field–flow fractionation and nanoflow ultrahigh performance liquid chromatography–tandem mass spectrometry, Anal. Chim. Acta 1073 (2019) 79–89.
[29] J.S. Yang, J.C. Lee, S.K. Byeon, K.H. Rha, M.H. Moon, Size dependent lipidomic analysis of urinary exosomes from patients with prostate cancer by flow field-flow fractionation and nanoflow liquid chromatography-tandem mass spectrometry, Anal. Chem. 89 (2017) 2488–2496.
[30] Y.B. Kim, G.B. Lee, M.H. Moon, Size separation of exosomes and microvesicles using flow field-flow fractionation/multiangle light scattering and lipidomic comparison, Anal. Chem. 94 (2022) 8958–8965.
[31] S.K. Wiedmer, M.-L. Riekkola, Field-flow fractionation-an excellent tool for fractionation, isolation and/or purification of biomacromolecules, J. Chromatogr. A 464492 (2023).
[32] H. Zhang, et al., Identification of distinct nanoparticles and subsets of extracellular vesicles by asymmetric flow field-flow fractionation, Nat. Cell Biol. 20 (2018) 332–343.
[33] V. Marassi, B. Roda, A. Zattoni, M. Tanase, P. Reschiglian, Hollow fiber flow field-flow fractionation and size-exclusion chromatography with multi-angle light scattering detection: a complementary approach in biopharmaceutical industry, J. Chromatogr. A 1372 (2014) 196–203.
[34] M. Tanase, et al., Role of carbonyl modifications on aging-associated protein aggregation, Sci. Rep. 6 (2016) 19311.
[35] V. Marassi, et al., A new approach for the separation, characterization and testing of potential prionoid protein aggregates through hollow-fiber flow field-flow fractionation and multi-angle light scattering, Anal. Chim. Acta 1087 (2019) 121–130.
[36] V. Marassi, et al., An ultracentrifugation–hollow-fiber flow field-flow fractionation orthogonal approach for the purification and mapping of extracellular vesicle subtypes, J. Chromatogr. A 1638 (2021) 461861.
[37] V. Marassi, et al., Emerging microfluidic tools for simultaneous exosomes and cargo biosensing in liquid biopsy: new integrated miniaturized FFF-assisted approach for colon cancer diagnosis, Sensors 23 (2023) 9432.
[38] M. Magatti, S. Pianta, A. Silini, O. Parolini, Isolation, culture, and phenotypic characterization of mesenchymal stromal cells from the amniotic membrane of the human term placenta, Mesenchymal Stem Cells: Methods and Protocols (2016) 233–244.
[39] D. Rossi, S. Pianta, M. Magatti, P. Sedlmayr, O. Parolini, Characterization of the Conditioned Medium from Amniotic Membrane Cells: Prostaglandins as Key Effectors of its Immunomodulatory Activity, 2012.
[40] M. Dominici, et al., Minimal criteria for defining multipotent mesenchymal stromal cells. The International Society for Cellular Therapy position statement, Cytotherapy 8 (2006) 315–317.
[41] O. Parolini, et al., Concise review: isolation and characterization of cells from human term placenta: outcome of the first international Workshop on Placenta Derived Stem Cells, Stem Cell. 26 (2008) 300–311.
[42] A.R. Silini, et al., Perinatal derivatives: where do we stand? A roadmap of the human placenta and consensus for tissue and cell nomenclature, Front. Bioeng. Biotechnol. 8 (2020) 1438.
[43] P. Reschiglian, et al., On-line hollow-fiber flow field-flow fractionation-electrospray ionization/time-of-flight mass spectrometry of intact proteins, Anal. Chem. 77 (2005) 47–56.
[44] R. Mildner, et al., Improved multidetector asymmetrical-flow field-flow fractionation method for particle sizing and concentration measurements of lipid-based nanocarriers for RNA delivery, Eur. J. Pharm. Biopharm. 163 (2021) 252–265.
[45] ISO/TS 21362, 2018.
[46] V. Marassi, et al., FFF-based high-throughput sequence shortlisting to support the development of aptamer-based analytical strategies, Anal. Bioanal. Chem. 14 (18) (2022) 5519–5527.
[47] A. Zattoni, E. Loli Piccolomini, G. Torsi, P. Reschiglian, Turbidimetric detection method in flow-assisted separation of dispersed samples, Anal. Chem. 75 (2003) 6469–6477.
[48] J.C. Giddings, J.Y. Frank, N.M. Marcus, Theoretical and experimental characterization of flow field-flow fractionation, Anal. Chem. 48 (8) (1976) 1126–1132.
[49] S. Dubascoux, F. Von Der Kammer, I. Le Hécho, M.P. Gautier, G. Lespes, Optimisation of asymmetrical flow field flow fractionation for environmental nanoparticles separation, J. Chromatogr. A 1206 (2008) 160–165.
[50] V. Marassi, et al., Native study of the behaviour of magnetite nanoparticles for hyperthermia treatment during the initial moments of intravenous administration, Pharmaceutics 14 (2022) 2810.
[51] S. Rontogianni, et al., Proteomic profiling of extracellular vesicles allows for human breast cancer subtyping, Commun. Biol. 2 (2019) 325.
[52] U. Distler, J. Kuharev, P. Navarro, S. Tenzer, Label-free quantification in ion mobility–enhanced data-independent acquisition proteomics, Nat. Protoc. 11 (2016) 795–812.
[53] J.R. Wiśniewski, A. Zougman, N. Nagaraj, M. Mann, Universal sample preparation method for proteome analysis, Nat. Methods 6 (2009) 359–362.
[54] E.W. Deutsch, et al., Human proteome project mass spectrometry data interpretation guidelines 3.0, J. Proteome Res. 18 (2019) 4108–4116.
[55] A. Fabregat, et al., Reactome pathway analysis: a high-performance in-memory approach, BMC Bioinf. 18 (2017) 1–9.
[56] H. Mi, et al., PANTHER version 11: expanded annotation data from Gene Ontology and Reactome pathways, and data analysis tool enhancements, Nucleic Acids Res. 45 (2017) D183–D189.
[57] D. Szklarczyk, et al., STRING v11: protein–protein association networks with increased coverage, supporting functional discovery in genome-wide experimental datasets, Nucleic Acids Res. 47 (2019) D607–D613.
[58] V. Marassi, et al., Perspectives on protein biopolymers: miniaturized flow field-flow fractionation-assisted characterization of a single-cysteine mutated phaseolin expressed in transplastomic tobacco plants, J. Chromatogr. A 1637 (2021) 461806.
[59] V. Marassi, et al., An ultracentrifugation - hollow-fiber flow field-flow fractionation orthogonal approach for the purification and mapping of extracellular vesicle subtypes, J. Chromatogr. A 1638 (2021) 461861.
[60] R.R. Mizenko, et al., Tetraspanins are unevenly distributed across single extracellular vesicles and bias sensitivity to multiplexed cancer biomarkers, J. Nanobiotechnol. 19 (2021) 250.
[61] S. Singh, A. Numan, S. Cinti, Electrochemical nano biosensors for the detection of extracellular vesicles exosomes: from the benchtop to everywhere? Biosens. Bioelectron. 216 (2022) 114635.
[62] F. Iavarone, et al., Cryptides: latent peptides everywhere, Crit. Rev. Biochem. Mol. Biol. 53 (2018) 246–263.
[63] F. Trindade, et al., Salivary peptidomic as a tool to disclose new potential antimicrobial peptides, J. Proteonomics 115 (2015) 49–57.
[64] U. Kragh-Hansen, Possible mechanisms by which enzymatic degradation of human serum albumin can lead to bioactive peptides and biomarkers, Front. Mol. Biosci. 5 (2018) 63.
[65] K. Nakagomi, et al., Isolation of cathepsin B inhibitory peptides, Cabin-A1 and-A2, from a tryptic and chymotryptic hydrolysate of human serum albumin, Peptides 23 (2002) 1567–1571.
[66] O. Mijanović, et al., Cathepsin B: a sellsword of cancer progression, Cancer Lett. 449 (2019) 207–214.
[67] S. Gupta, A.K. Sharma, V. Shastri, M.K. Madhu, V.K. Sharma, Prediction of anti-inflammatory proteins/peptides: an insilico approach, J. Transl. Med. 15 (2017) 1–11.
[68] G. Sosne, P. Qiu, A.L. Goldstein, M. Wheater, Biological activities of thymosin ß4 defined by active sites in short peptide sequences, Faseb. J. 24 (2010) 2144–2151.